MEAN PRESSURE MEASUREMENTS OF MICRO-VORTEX GENERATOR AT MACH 2.5

by

YUSI SHIH

Presented to the Faculty of the Graduate School of
The University of Texas at Arlington in Partial Fulfillment
of the Requirements
for the Degree of

MASTER OF SCIENCE IN AEROSPACE ENGINEERING

THE UNIVERSITY OF TEXAS AT ARLINGTON

December 2010

Copyright © by YUSI SHIH 2010

All Rights Reserved

ACKNOWLEDGEMENTS

This is an exciting moment that I have finished my master's thesis. First of all, appreciation goes to my advisor, Dr. Frank Lu. Without his patience, enthusiasm, inspiration, expertise, guidance, and support in my research, I would never achieve this work. Dr. Lu led me to the experimental aerodynamics field, and ignited my enthusiasm towards this fascinating subject. Under his advice, my knowledge has grown by leaps and bounds Secondly, I am grateful to Dr. Don Wilson. Dr. Wilson is my graduate advisor and was very encouraging and very helpful. Dr. Wilson always gave me assistance when I had difficulties in school life and helped me to make right decisions. Also, I would like to thank Adam Pierce. Adam is my laboratory partner, and we did experiments together in the Aerodynamics Research Center. He is just like my older brother, always giving me help not only on my work but also on many things in life. Moreover, I wish to thank all the people at the Aerodynamics Research Center. It is because of them that we have such an dynamic, and friendly academic environment. A special thanks goes to Rodney Duke of the Aerodynamics Research Center and Howard Bailiff of the Physics Machine Shop, who are highly skilled in machining so many of my parts. Finally, I am indebted to my loving family in Taiwan, for their love, constant motivation and encouragement throughout my life. This work is funded by the Air Force Office of Scientific Research, through Grant No. FA9550-08-1-0201, monitored by Dr. John Schmisseur.

November 18, 2010

ABSTRACT

MEAN PRESSURE MEASUREMENTS OF MICRO-VORTEX GENERATOR AT MACH 2.5

YUSI SHIH, M.S.

The University of Texas at Arlington, 2010

Supervising Professor: Frank K. Lu

Shock wave/boundary layer interactions (SBLIs) are always an important issue for high-speed vehicles. SBLIs reduce the performance of aerodynamic surfaces and engine inlets, amongst a number of adverse effects. Micro-vortex generators (MVGs) are a potential flow control method that has seen intense investigation recently and have even been implemented in actual configurations at low speeds. The present research is focused on the mean pressures at Mach 2.5 around an MVG. Experiments were performed with a baseline flat plate and also with two MVG configurations (70 and 45 trailing edge) mounted ahead of a 5° ramp. In the present study MVGs are used to manipulated the flow within the boundary layer and the effects on the weak oblique shock produced by the 5° ramp are recorded. The results appeared similar to the large eddy simulations reported by Li and Liu [1] and [2]. Three conclusions can be made in present research

1. The different behaviors of SBLI, with MVG and without MVG, were observed from mean pressure measurements.

2. The mean pressure right behind MVG is lower, compared to the mean pressure in the middle of two MVGs.
3. The trailing angle of the MVG does affect the mean pressure distribution.

TABLE OF CONTENTS

LIST OF FIGURES

LIST OF TABLES

CHAPTER 1

INTRODUCTION

1.1 Background

1.1.1 SBLIs and MVG

The interaction of a shock wave with a boundary layer generally causes the performance of an aerodynamic surface to deteriorate, especially if the adverse pressure gradient of the interaction is sufficient to cause the boundary layer to separate. The interaction results in poor pressure recovery, intense heating and unsteadiness. A practical example would be in supersonic inlets where SBLIs can reduce the inlet's effective area and can even cause engine unstart. Various methods have been proposed for overcoming the adverse effects of SBLIs. A passive method that has been proposed recently is to use a sub-boundary layer device called micro-vortex generator (MVG). Compared to other flow control methods, such as boundary layer bleed, conventional VGs, Holden et al.[3] and Anderson et al.[4] argued that MVGs have a lower drag penalty and is effective in separation flow control. Ashill et al.[5] [6] also mentioned that MVGs can reduce the shock strength on transonic airfoils in some cases. Other than being found in research laboratories, MVGs have been found in many applications; for example, Micro AeroDynamics Inc. has commercial MVGs kits. The way that MVGs affects SBLIs is not yet clear; therefore, it is presently a hot topic of ongoing research. MVGs are thought to function similarly to conventional VGs in energizing the boundary layer via entrainment of the free stream flow by trailing vortices. The studies were initially at low speed and then extended to supersonic flow where research mainly focused on reducing the flow separation of strong SBLIs.

Some researchers, like Blinde et al.[7] even claimed that MVGs not only reduce the flow separation, but also that the length of shock motion can be reduced. Therefore, the way to generate such trailing vortices with an MVG can be regarded as a principle in controlling SBLIs. It appears that the behavior of the trailing vortices may be based on how the specific MVGs are designed. Previous experiments suggested several parameters for designing MVGs, such as the distance upstream of the shock impingement location,[8][9] spanwise spacing,[8],[10] and geometric parameters such as size and height.[3],[7],[8],[11]. In the present research, the design of MVGs was based on that of Li and Liu.[2],[1] A ramp-type MVG, 2 mm high, was utilized in the present experiment. Also, the MVG had two different trailing edge angles of 70 and 45 to study their effect. Nevertheless, there were two differences between Li and Liu's study[2],[1] from the present research, namely, the MVG array design and oblique shock wave generator design (ramp angle). For Li and Liu, there was only one MVG, but there were five MVGs forming an array in the present design. Moreover, Li and Liu had a 24 leading edge ramp downstream of the MVG but the present study had a 5 ramp. The primary reason that Li and Liu had only one MVG is computational limitations. For the experimental work, extra MVGs do not pose additional difficulties. Thus, the experiments were designed with a baseline without MVGs and with two MVG configurations, with or without the 5 ramp to give a total of six cases.

1.1.2 Mean Pressure Measurements

Mean pressure measurements were used to study how MVGs affect SBLIs by manipulating the upstream flow. Mean pressure measurements in the present research were obtained at Mach 2.4.[12] Either an array of MVG70 or MVG45 was mounted ahead of a 5 ramp which produced a weak, unseparated SBLI at Mach 2.5. The boundary layer thickness was about 4 mm and Reynolds number based on the boundary layer thickness was 1.6 million/m.[12]

CHAPTER 2

EXPERIMENTAL SETUP

Experiments were performed in the blow down supersonic wind tunnel in the Aerodynamics Research Center (ARC) at UTA. The facility generates flows in the Mach number range of 1-4, in a test section of dimensions 15.2 cm^2 81.28 cm long. Details of the wind tunnel can be found in Matsumoto.[13]

2.1 Air supply system and wind tunnel

The air was compressed and dried for testing. A Clark Dresser 5-stage compressor is available for this purpose. The five stages raised the ambient air to 0.2, 0.83, 3.45, 6.89, 13.8 MPa (30, 120, 500, 1000 and 2000 psi). Due to storage bottles being rated at 2000 psi, the compressor was derated to that level. During compression, water and oil in the air were condensed and flowed out of a drain. In addition, the air was dried by a twin-tower drier and the dewpoint was measured by a Vaisala dewpoint meter. A dewpoint of about - $40C^\circ$ is required for supersonic wind tunnel testing.[14]

Air from the $13.8MPa(2000psi)$ tanks was passed to two storage vessels with a total volume of 1.8 m^3 located immediately upstream of the wind tunnel. The auxiliary storage vessels were rated to $5.17MPa(750psi)$. For the present experiments, the pressure in the auxiliary storage vessels was kept at $2.34MPa(340psi)$.

Three valves were located downstream of the storage vessels Fig. 2.1. The first and the second are a Velan manual gate valve and a lever handle, which were opened prior to operating the tunnel. The third is a Fisher Controls pneumatically operated control valve. The valve is $15.24cm(6in.)$ in diameter and is driven by a

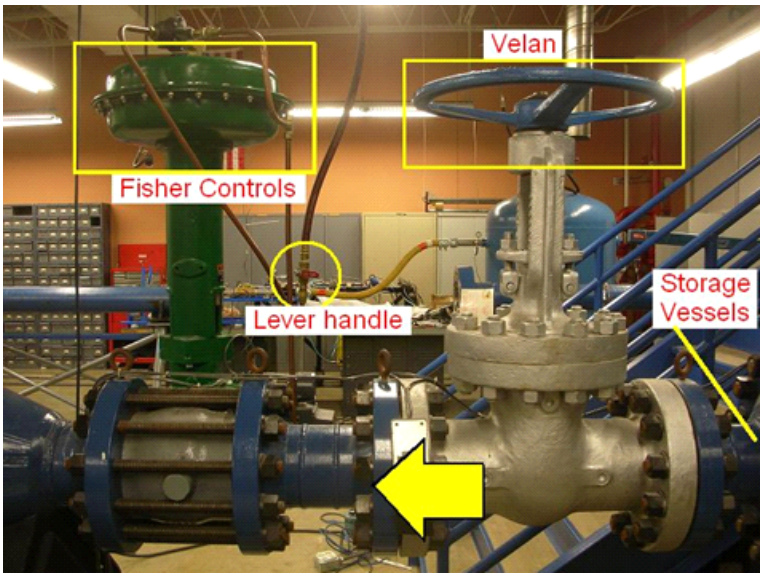

Figure 2.1. The Flow control valves.

$1.38MPa(200psi)$ supply. This valve was controlled by a PC with a custom LabVIEW program.

2.2 Test Section

A CAD rendition of the test section designed by previous student Mitchell is shown in Fig. 2.2. The flow direction is from left to right as indicated by the yellow arrow. The nozzle and the diffuser are located at the left and right sides of the test section respectively. The test section is outfitted with extensive optical access from both sides and from the top. The two sides can be taken off for configuration changes. Normally, each of them is butted tightly to the test section with 44 screws. The top is removable as well and is secured by 40 screws. For configuration changes, there is no need to remove the top.

2.2.1 Test Platform

The test platform consisted of a flat plate that was made in layers, where the top layer was made of a number of small, thin plates secured tightly together to

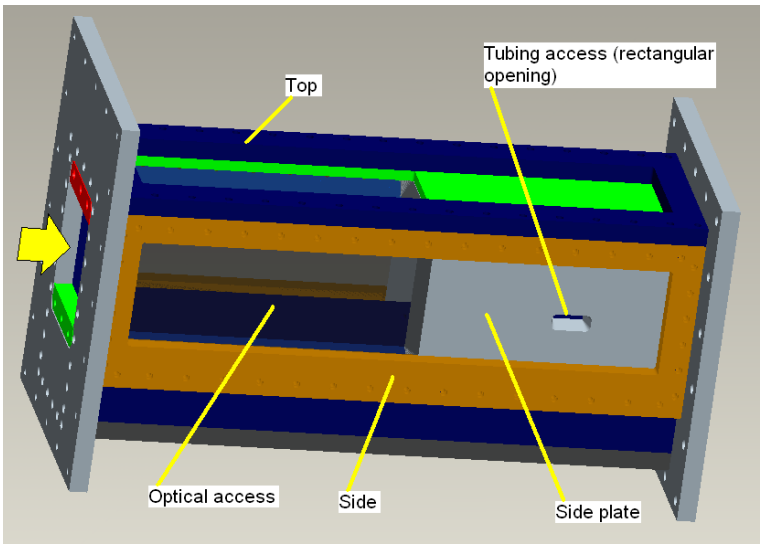

Figure 2.2. CAD rendition of test section.

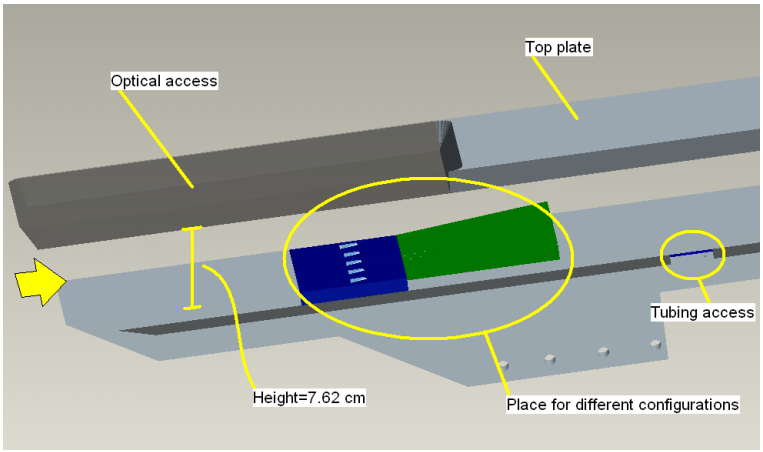

Figure 2.3. CAD rendition of test platform assembly.

form a continuous, flat surface. This modular design allowed for quick configuration changes. Figure 2.3 displays the assembly of the test platform; see section 2.2.4 for more configurations. The height from the surface of the test platform to the ceiling of the test section is 7.62 cm (3 in.). Most parts of test platform were made of aluminum 6061, except the 70MVG and 45MVG plates.

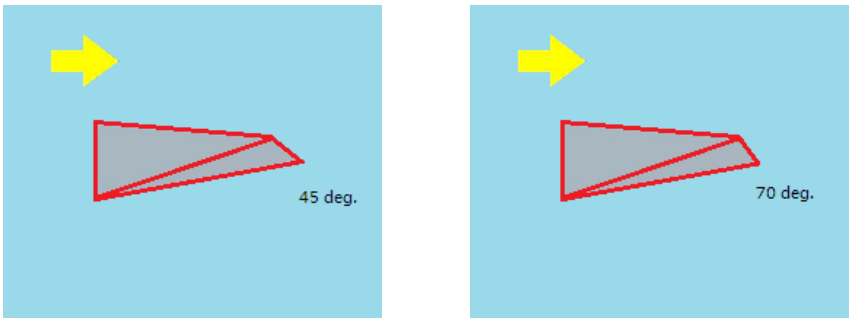

(a) (b)

Figure 2.4. CAD rendition of MVG element (a) 45MVG (b) 70MVG.

2.2.2 Micro-ramp vortex generator

Unlike the vertical trailing edge of Babinsky et al.[9] and most previous investigators, the present MVG design has trailing edges inclined at 45 and 70 from the base plane. The shape of a single MVG is shown in Fig. 2.4(a). In the figure, the leading edge is on the left. The height of each MVG is 2 mm (0.079 in.), representing about 50% of the height of the boundary layer (3-4 mm).13 Each MVG is 12.95 mm (0.51 in.) long. The front of each MVG is 11.7 mm (0.46 in.) wide and the angle of the leading edge is 8.

2.2.3 MVG plate and oblique shock wave generator(ramp)

Figure 2.5 shows the MVG plate insert. The MVG inserts consist of an array of five single MVGs arranged spanwise. These inserts were made by C and F Tooling Dallas, Texas where the array was formed by grinding an S7 steel plate. The center-to-center spacing between the MVGs is 30.5 mm (1.2 in.). The two side MVGs were at a distance of 15.2 mm (0.6 in.) from the edges. The leading edge of the MVG array was located 272 mm (10.7 in.) downstream of the leading edge of the test platform, see Figs. 2.8 and 2.9. In addition, Fig. 2.5 shows surface taps for pressure measurements. Further discussion of the pressure taps are found in section 2.3.1.

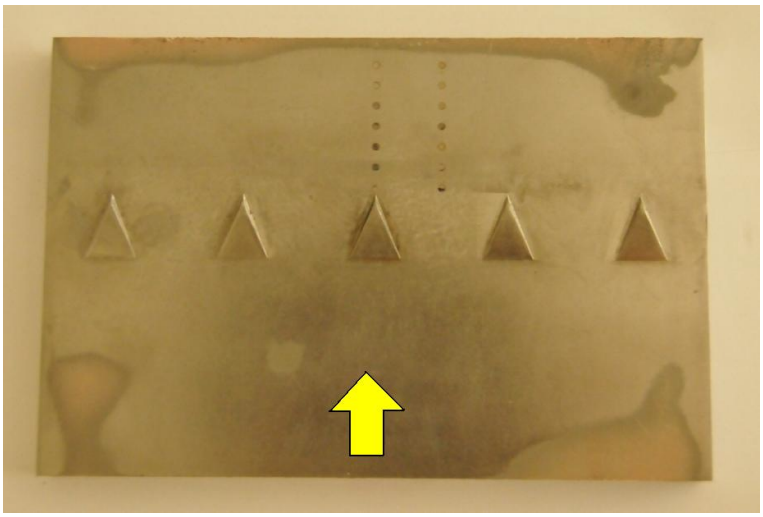

Figure 2.5. Plate insert showing the five MVG array.

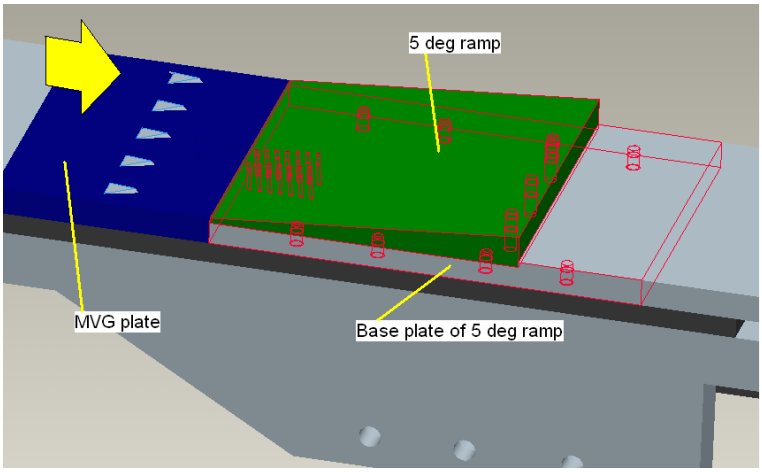

Figure 2.6. CAD rendition of ramp plate.

A shock generator in the form of a two-dimensional 5 ramp is shown in Fig. 2.6. The ramp was made of 6061 aluminum. This ramp had three threaded holes on its bottom which allows it to be tightly mounted on its own base plate; see the red highlight in Fig. 2.6 and also appendices A.3 and A.4. The whole assembly was then mounted flush with the entire flat plate to form a single assembly.

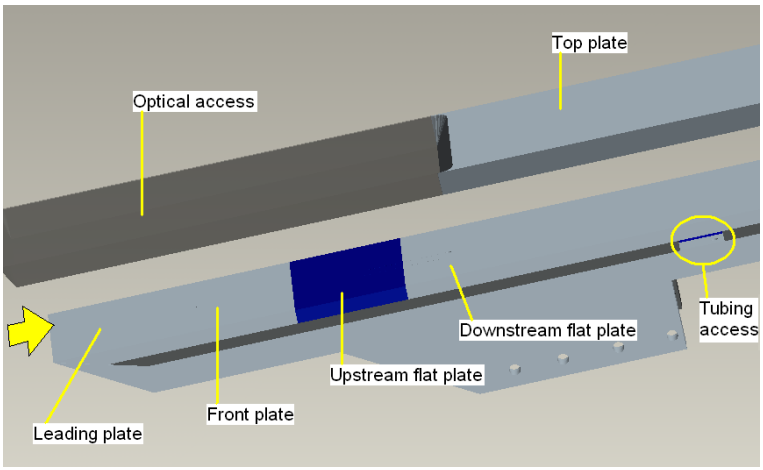

Figure 2.7. CAD rendition of "'All Flat"' assembly.

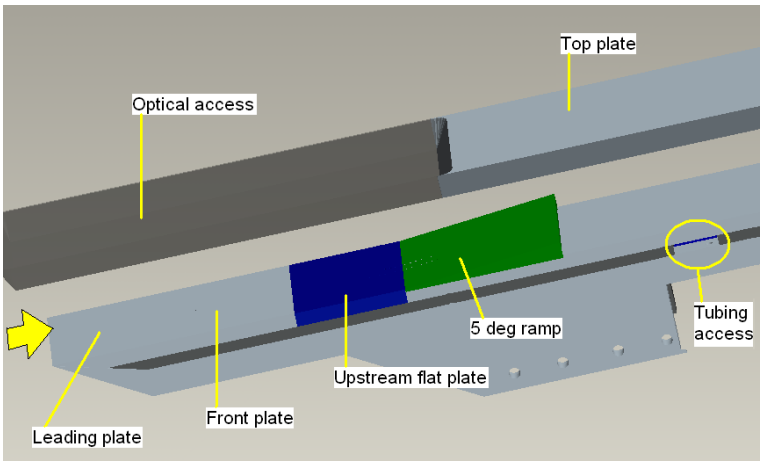

Figure 2.8. CAD rendition of "'NoMVG+Ramp"' assembly.

2.2.4 Assembly

The combination of no MVG, 70MVG and 45MVG with or without the 5 ramp yielded a total of six configurations, which are shown in the CAD renditions of Figs. 2.7-2.10. Figure 2.7 shows the flat plate which is the baseline "All Flat" configuration. Figure 2.8 shows the "NoMVG+Ramp" configuration. This configuration is formed with the leading plate, the front plate, the upstream flat plate, and the 5 ramp plate. The height from the top edge of the 5 ramp to the test section ceiling is 6.35 cm (2.5

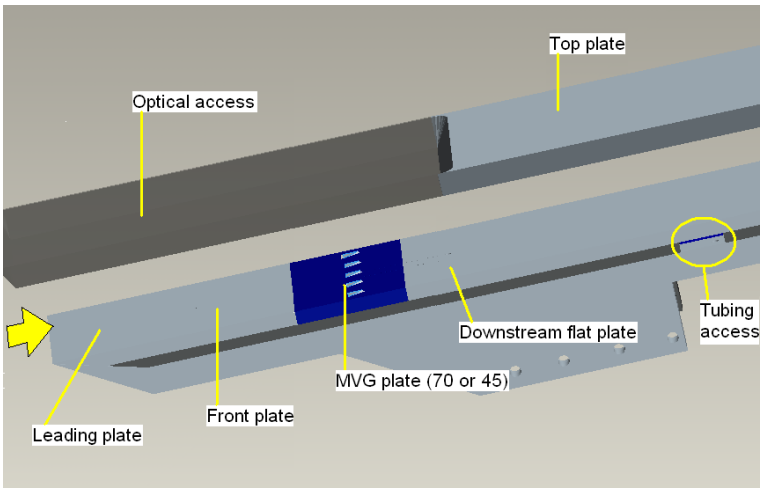

Figure 2.9. CAD rendition of "'MVG+Flat"' assembly.

in.) and the distance from the leading edge of the leading plate to the leading edge of ramp plate is 32.38 cm (12.75 in.). The "MVG+Flat" configuration is displayed in Fig. 2.9. This configuration is composed of the leading plate, the front plate, the MVG plate (70MVG or 45MVG), and the downstream plate. Again, the distance from the leading edge of the leading plate to the leading edge of the MVGs is 27.2 cm (10.7 in.) The last configuration, "MVG+Ramp," is shown in Fig. 2.10 and it is made up of the leading plate, the front plate, the MVG plate (70MVG or 45MVG), and the 5 ramp.

2.3 Pressure measurements

2.3.1 Pressure taps

Surface pressure measurements were made in two rows parallel to the incoming free stream direction, namely the center and side rows (C and S, respectively) depending on their location with respect to the central MVG location, shown in Fig. 2.11. Row C is along the centerline of the configuration and row S is 1.52 cm (0.5 in.) away from C, that is, it is half of the spanwise distance between two MVGs. These measurements help in developing an understanding of the effect of MVGs on

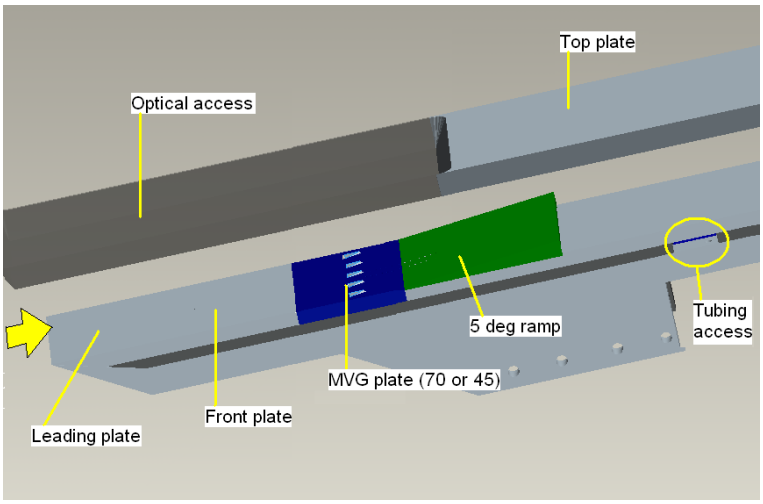

Figure 2.10. CAD rendition of "'MVG+Ramp"' assembly.

the flow. Each row has 15 taps. Additionally, a reference tap is located at 11.43 cm (4.5 in.) downstream of the leading edge of the leading plate for a total of 31 taps. The pressure tap distribution for each plate segment is as follows:

1. 70MVG or 45MVG plate (Appendix A.2): Two rows totaling 16 taps (8 taps per row, Fig. 2.11). These taps were made by electrical discharge machining by Bailey Tool and Manufacturing, Duncanville, Texas.
2. Ramp plate (Appendices A.3 and A.4): Two rows with a total of 14 taps (7 taps for each row, Fig. 2.11). These taps are perpendicular to the ramp surface (Fig.2.13).
3. Upstream flat plate (Appendix A.2, Fig. 2.12) with 16 taps (8 for C, 8 for S), machined in ARC.
4. Downstream flat plate (Appendix A.7, Fig. 2.12) with 14 taps (7 for C, 7 for S), machined in ARC.
5. Front plate (Appendix A.5, Fig. 2.11 and 2.12): one reference tap machined in Physics Machine Shop.

The diameter of all the taps is 1.7 mm (0.067 in.) in order to fit Kulite pressure transducers (but which were not used in present experiment).

The taps along a row are labeled as No.1, 2, 3, , 16 with distance downstream. For example, tap No.1 is the reference, tap No. 2 is the tap right behind the MVG, tap No.9 is the first tap on the ramp plate, and tap No.16 is the last one on the ramp plate. Figure 2.13 displays the side view of a pressure row, with 8 taps on the MVG plate and 7 taps on the ramp plate. Note that rows C and S are overlapped in this side view. Figure 2.14 (see also Appendices A.2, A.3, and A.4) displays the spacings among all 15 taps along a row: They are equally spaced at 4.83 mm16,17 (0.19 in.), except tap No. 2 which is 1.44 mm (0.06 in.) from the downstream tip of the MVG. Hence, tap No. 3 is 6.28 mm (1.44 + 4.83 1 mm) away from the downstream tip of the MVG, tap No. 4 is 11.11 mm (1.44 + 4.83 2 mm), and so on. Taps No.10-16 are on the ramp and are also spaced at 4.83 mm. Therefore, tap No. 10 is 40.09 mm (1.44 + 4.83 8 mm) and tap No.11 is 44.92 mm (1.44 + 4.83 9 mm) from the downstream tip of the MVG, etc.

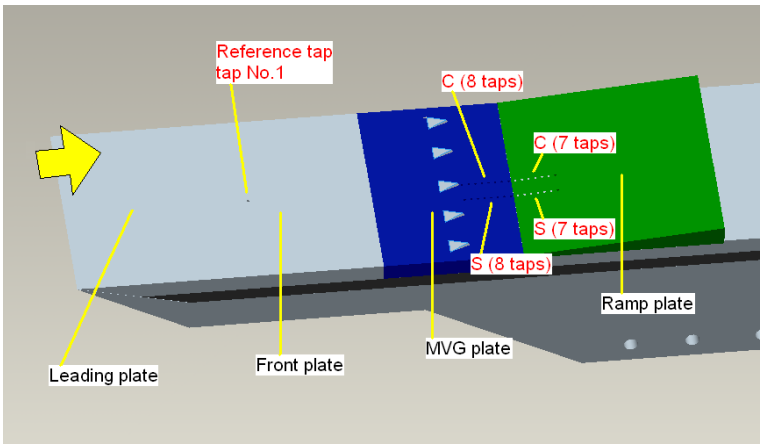

Figure 2.11. CAD rendition of pressure taps distribution on MVG plates and ramp plate.

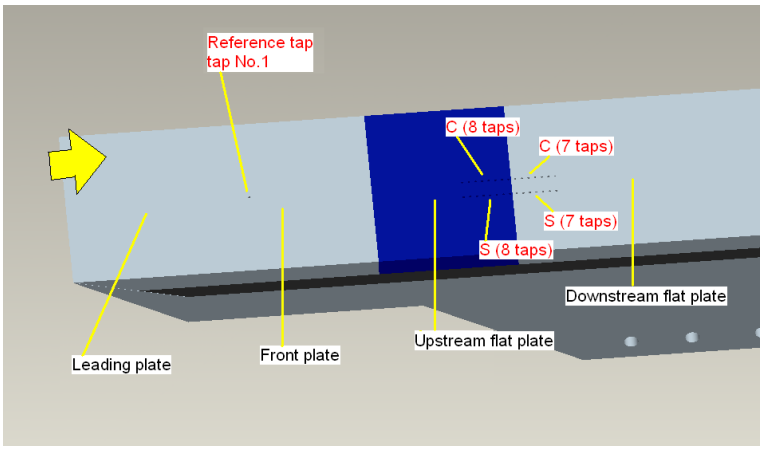

Figure 2.12. Pressure taps distribution on upstream and downstream flat plates.

2.3.2 Pressure scanner and its calibration

According to perfect gas assumption, knowing the total pressure P_0 and the Mach number, the static pressure P_1 can be calculated from the isentropic flow relation:

$$\frac{P_0}{P_1} = \left(1 + \frac{\gamma - 1}{2} M^2\right)^{\frac{\gamma}{\gamma - 1}} \tag{2.1}$$

With $P_0 = 473.6$ kPa (68.34 psia), P_1 at a test section Mach number of 2.5 is 27.6 kPa (4 psia). Next, consider the oblique shock relation:

$$\beta = \arctan \frac{M^2 - 1 + 2\lambda \cos \frac{4\pi + \arccos \chi}{3}}{3\left(1 + \frac{\gamma - 1}{2} M^2\right) \tan \theta} \tag{2.2}$$

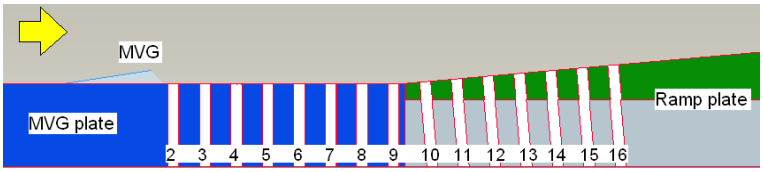

Figure 2.13. CAD rendition the side view of a pressure row.

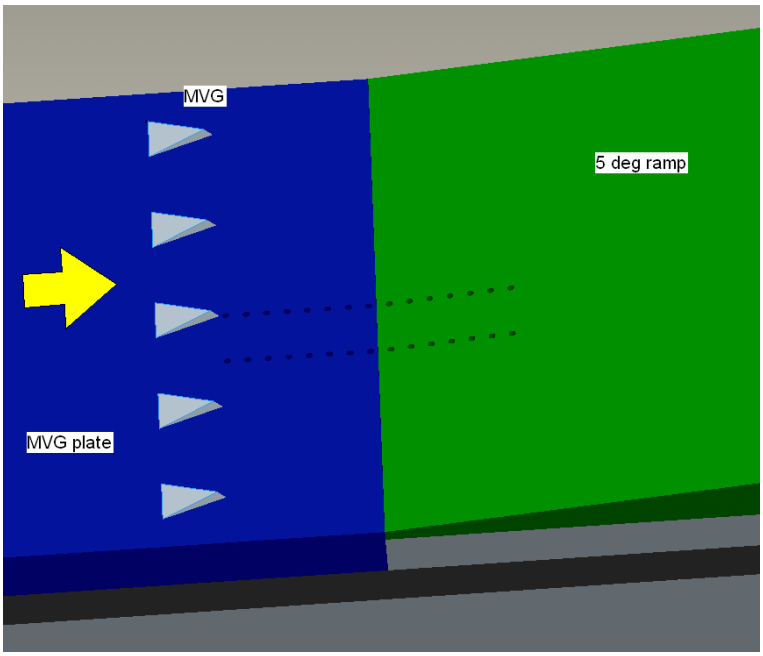

Figure 2.14. CAD rendition of pressure taps distribution.

$$\lambda = \sqrt{\left(M^2-1\right)^2 - 3\left(1+\frac{\gamma-1}{2}M^2\right)\left(1+\frac{\gamma+1}{2}\right)\tan\theta^2} \tag{2.3}$$

$$\chi = \frac{\left(M^2-1\right)^3 - 9\left(1+\frac{\gamma-1}{2}M^2\right)\left(1+\frac{\gamma-1}{2}M^2+\frac{\gamma+1}{4}M^4\right)\tan\theta^2}{\lambda^3} \tag{2.4}$$

Substituting M = 2.5 and $\theta = 5°$ yields the shock angle $\beta = 27.4°$. With P_1 and β, the pressure ratio across the oblique shock, given by

$$\frac{P_2}{P_1} = 1 + \frac{2\gamma}{\gamma+1}\left((M\sin\beta)^2 - 1\right) \tag{2.5}$$

Yielding $P_2 = 38.1$ kPa (5.52 psia). Therefore, given that the static pressure and, thus, the wall pressures for the present experiments range from 27.6-38.1 kPa (4-5.52 psia), a sub-atmospheric pressure calibration system is necessary. An Esterline NetScanner Model 9116 Ethernet Intelligent Pressure Scanner18 (Fig. 2.15) with 0.05% full-scale accuracy was utilized for pressure measurements in the present experiments. Sixteen pressures can be scanned and all the sensors can be connected to those 16 pressure taps on the test platform. Calibration of the NetScanner was done against a MKS Baratron pressure transducer type 227AA-01000B power supply and digital readout unit. The calibration range is from atmosphere 101 kPa (14.6 psia) down to 31.7 kPa (4.6 psia), and it was achieved by a Boekel Hyvac vacuum pump. A cylinder metal container with two ports was used as a sub-atmospheric chamber for pressure transducer calibration, see Fig. 2.16. Two tee fittings were hooked on the two ports of the container. The Baratron and the Boekel Hyvac were connected to one tee (upper portion of Fig. 2.16). The pressure release valve (shown in gray in the figure) and the regulator (which connects to the NetScanner) were linked to the other tee (On the lower of Fig. 2.16). Figure 2.17 shows the regulator with eight switches on it to facilitate the calibration of each single sensor of NetScanner.

The calibration was done while all the switches of the regulator were on. Thus, all 16 readings on NetScanner should be the same, theoretically. However, the 16 sensors produced slightly different readings. Table 2.1 shows the sensitivity of each sensor.

The calibration was performed from 101 kPa (14.6 psia) to 31.7 kPa (4.6 psia) at increments of about 1 psi. An example result is shown in Fig. 2.18. The pressure relationship of the NetScanner sensors and the Baratron transducer is extremely linear. The deviation (see Fig. 2.19) is only 0.1103 kPa (0.016 psi) on the NetScanner axis so it can barely be seen in Fig. 2.18.

Figure 2.15. Esterlin NetScanner.

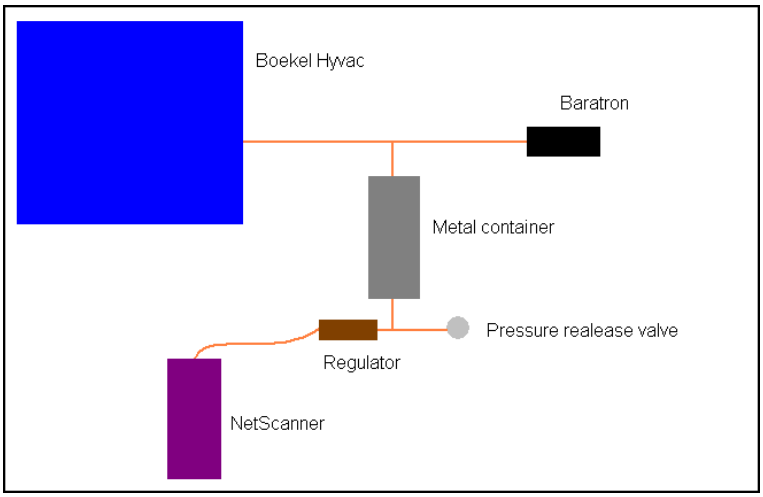

Figure 2.16. The sub-atmosphere calibration system.

In summary, the calibration procedure is as follows:

1. Connect NetScanner, pressure release valve, Baratron, and Boekel Hyvac to the cylindrical metal container
2. Close the pressure release valve, and ensure that everywhere in the system is sealed.

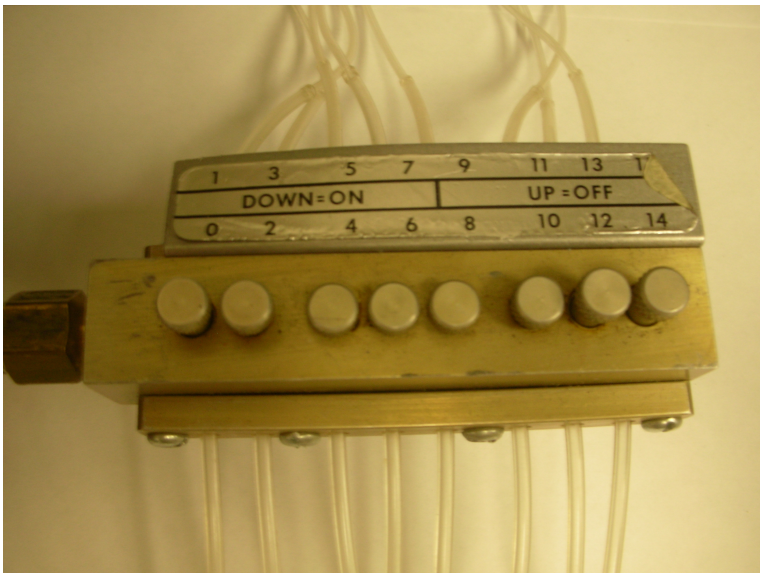

Figure 2.17. Regulator.

Table 2.1. Sensitivity of the NetScanner sensor

Sensor	Sensitivity psi/kPa	Offset	R^2	Accuracy
1	.01453/1.0018	-14.283	1	±0.02
2	.01453/1.0018	-14.283	1	±0.04
3	.01453/1.0018	-14.283	1	±0.02
4	.01453/1.0018	-14.283	1	±0.02
5	.01453/1.0018	-14.283	1	±0.02
6	.01453/1.0018	-14.283	1	±0.02
7	.01453/1.0018	-14.283	1	±0.03
8	.01453/1.0018	-14.283	1	±0.03
9	.01453/1.0018	-14.283	1	±0.02
10	.01453/1.0018	-14.283	1	±0.04
11	.01453/1.0018	-14.283	1	±0.02
12	.01453/1.0018	-14.283	1	±0.02
13	.01453/1.0018	-14.283	1	±0.03
14	.01453/1.0018	-14.283	1	±0.02
15	.01453/1.0018	-14.283	1	±0.03
16	.01453/1.0018	-14.283	1	±0.03

3. Turn on the Baratron.

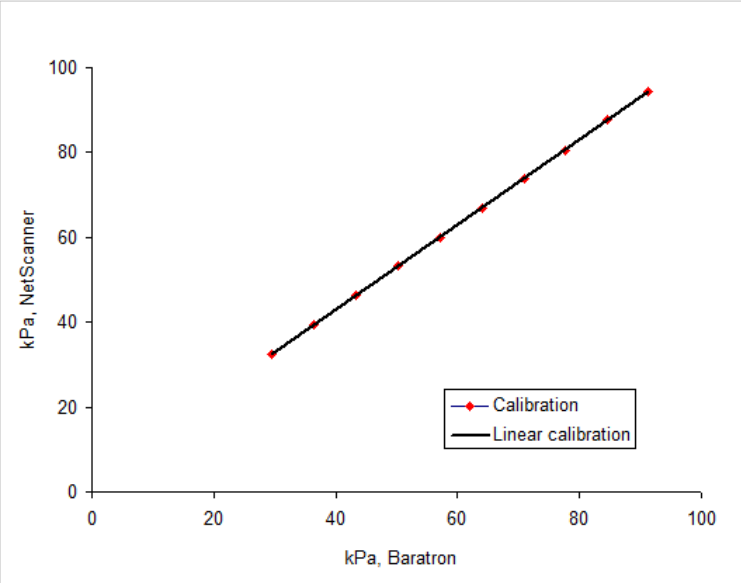

Figure 2.18. Typical calibration of Netscanner.

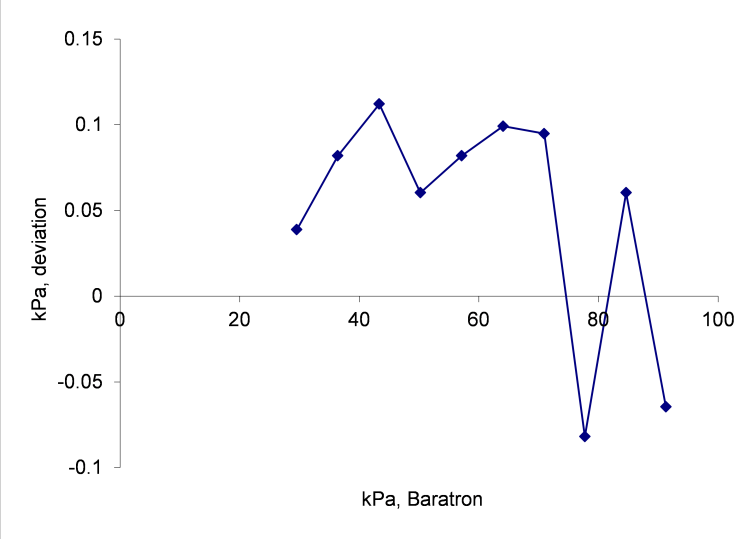

Figure 2.19. The deviation of calibration data.

4. Connect NetScanner to Ethernet of a computer with its own interface cable, set up the TCP/IP as the user IP and key in the addresses, and then turn on the NetScanner program
5. Turn the Boekel Hyvac on and start calibrating.

2.3.3 Pressure measurements

Access to the pressure taps from the externally mounted NetScanner was made by a rectangular opening on the right side of the test section (looking downstream) 4.06 cm long by 0.95 cm wide ($1.6 \times 0.375 in.$). Besides, a rubber plug (Fig. 2.22) was made to seal the 4.06 by 0.95 cm opening. The rubber plug is made of ReproRubber Thin Pour 130ml kits from Flexbar Machine Co. Fast and convenient, one can make a rubber plug by following the procedure:

1. Prepare 16 thin steel tubes of the length 4.06 cm (1.6 in.).
2. Insert these 16 thin steel tubes into an aluminum mold.
3. Pour the ReproRubber Thin Pour liquid into the mold and allow it to cure for about 15 minutes.
4. After curing, the plug is ready for experiment.

Figure 2.20 shows a long narrow cavity underneath the top layer outlined in red. This cavity was for housing and channeling tubing and wiring. The bottom cover plate (shown in blue) protects the tubing. Also, for a tube to access the reference Table 2.1, a small access of 0.30 cm long by 0.71 cm wide ($0.12 \times 0.28 in.$) on the U shape plate was made (Fig. 2.21). Tygon tubes with 2.38 mm OD (2.38 mm, 3/32 in. OD. 0.79 mm, 1/32 in. ID) and Chemi tubes with 1.59 mm OD (1.58 mm, 2/32 in. OD. 0.79 mm, 1/32 in. ID) were used for pressure tubing. The reason for using tubes of different OD is that the taps on the S7 steel plates (the two MVG plates) were slightly larger than taps on the aluminum 6061 plates (all other plates). Tygon tubes were then used to connect these stainless steel tubes to the pressure scanner.

1. 8 Tygon tubes connected with stainless steel tubes (OD 1.59 mm, 1 cm long) are inserted to the pressure taps on the MVG plate and are attached by GE silicone sealant before the MVG plate is secured to the test platform. Normally, GE silicone takes 7–8 hours to be completely dry.

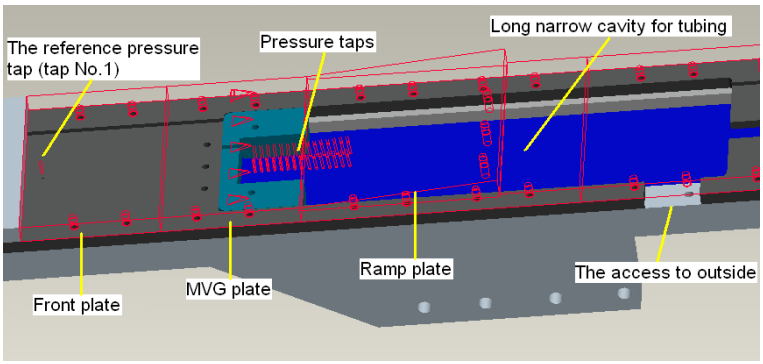

Figure 2.20. CAD rendition of implement of pressure measurments.

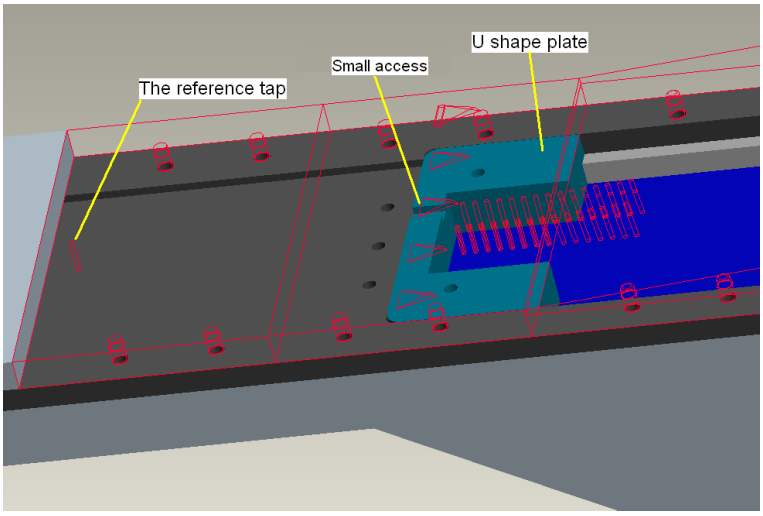

Figure 2.21. CAD rendition of the U shape plate and its small access to tube the reference tap 2.1.

2. After the MVG plate is secured on the test platform and the test platform is placed into the test section, the rubber plug is inserted in the rectangular opening and then the Tygon tubes are connected to the manifold on the rubber plug.
3. The cover plate at the bottom of the test platform is fastened to protect the pressure tubing from the supersonic flow.
4. Another 8 Tygon tubes are connected to the manifold outside of the test section to the NetScanner.

Figure 2.22. Rubber plug.

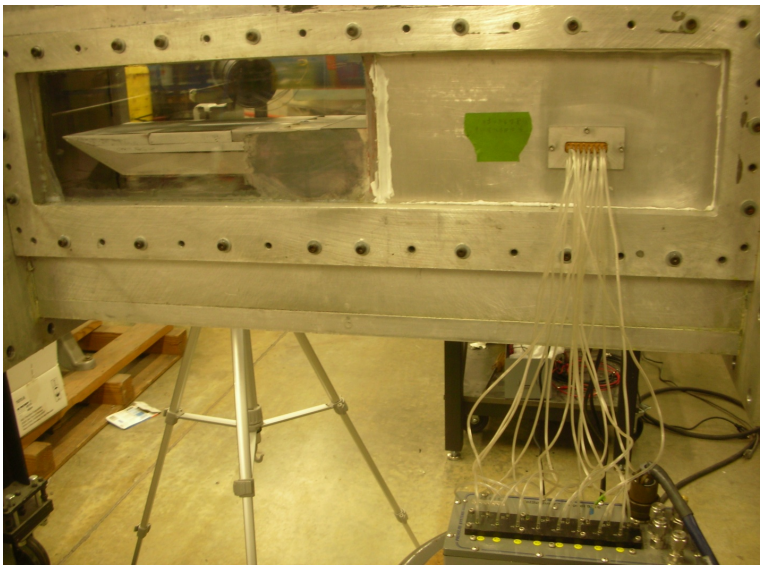

Figure 2.23. Outside view of pressure tubing.

The procedure of connecting the 7 Chemi tubes was similar, except these Chemi tubes were connected to one pressure row on the ramp plate (or downstream flat plate). Also, one Chemi tube is connected to the reference Table 2.1 on front plate. Figure 2.23 displays the outside view of the pressure tubing.

2.3.4 Pressure Scanner operation and collcetion

The NetScanner offers its own software, NUSS, for operation.[15] The NUSS software was operated in the record mode. Figure 2.24 shows the record mode. The pressure readings of 16 sensors are at the left column in psig. The gray column in the middle and the right column are the sampling rate and temperature respectively. The sampling rate can be up to 500 per second per channel. In the present experiment, the time interval of the records was set as 0.5 s. In the lower middle side of Fig. 2.24, a "Rec" button can be seen. With a click on it, the NUSS will start recording the pressures from the 16 sensors. Another click on the "Rec" stops recording. All data were recorded in DAT files and NUSS provides a function to transfer them into EXCEL files. In order to convert the files, a re-start of NUSS was necessary. Then, the playback mode was entered (Fig. 2.25) and the desired data to be transferred was chosen. Clicking on the box next to the "play" button (Fig. 2.25(a)), will show all the recorded data in a pop-up dialog box. Then choose the data to be transferred. Clicking the "play" button now allows the playback mode to allow all the data to be transferred (Fig. 2.25(b)).

2.3.5 Test Procedure

Due to the facility limit (only one NetScanner in ARC), only one pressure row was used. The other row was sealed by GE silicone sealant. All the taps in the other row were sealed flush to the surface. The procedure to run the experiments is as follows:

1. Turn on the 1.38 MPa (200 psi) compressor.
2. Open the valve connected to the 1.38 MPa (200 psi) compressor for calibrating the pneumatically operated control valve.12 For safety, the manual gate valve

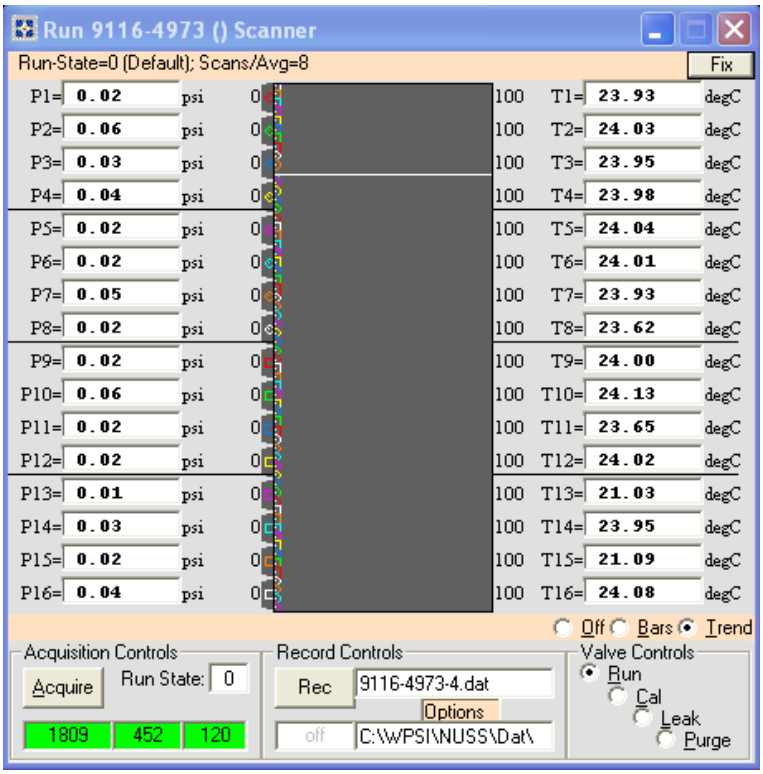

Figure 2.24. Record mode of NUSS.

(a) (b)

Figure 2.25. Playback mode of Nuss (a) The playback dialog bod of NUSS and (b) Playback mode of NUSS.

remains closed before opening the lever handle valve. Close the lever handle valve after calibrating.

3. Anchor down the wind tunnel (4 places).
4. Open the manual gate valve and the lever handle valve.
5. Start the LabVIEW control program12 and NetScanner program.
6. Run the wind tunnel to gather data.

CHAPTER 3

DISCUSSION

3.1 Possible error source

3.1.1 Flow quality

Flow quality affects the accuracy of pressure measurements. There are two major sources of error related to flow quality, namely, the compressed air and the tunnel operation. For the first concern, routine maintenance is important. Any contaminants such as oil or vapors in the air can cause pressure abnormalities. Secondly, a constant stagnation plenum pressure and a precise test section Mach number are required. For the second concern, the plenum pressure should be kept constant despite a decrease in the storage pressure. Fung et al.[16] suggested PI control for this purpose, where the conservation of mass, conservation of energy, and the universal gas sizing equation are utilized for estimating the pressure, mass flow, and pneumatic valve opening angle in both storage vessels, and plenum chamber. With the controller proportional gain K_p and the controller integral gain K_i combined properly, one can trace the poles in the complex domain to find steady-state solutions for controlling the pneumatic valve, so as to keep a constant pressure in the plenum chamber during the run. Braun et al.[17] developed an EXCEL simulation of the PI controller. In Fig. 3.1, the simulation with improper K_p shows unfavorable fluctuation of plenum pressure. In Fig. 3.2, a plenum pressure delay is displayed with an inappropriate K_i. A proper K_p and K_i combination for the desired stagnation pressure 517 kPa (75 psi) was found to be K_p=0.00005 and K_i=0.8, shown in Fig. 3.3. The storage pressure decreases continuously while the plenum pressure builds up and levels off to

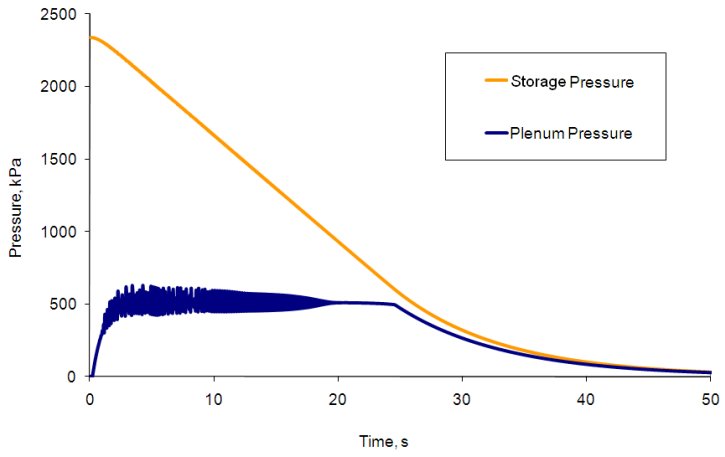

Figure 3.1. Storage and plenum pressure vs time, Mach 2.5 simulation (improper $K_p = 0.00007$).

the preset value. Eventually, at about 28 s after tunnel start, the storage pressure is too low to maintain the constant plenum pressure so the conditions allow for test duration of about 20 s. Note that the plenum pressure achieved is not truly constant because of the property of PI control. But from this simulation, we can obtain an better idea of the tunnel operation.

In reality, the nonlinear relations of gas flow and valve opening are the dynamics of the pneumatic valve during a run. The plenum pressure of 517 kPa (75 psi) should be attained as fast as possible so as not to waste the stored air. Thus, rapid opening of the control valve is desirable. Details can be referred to in Pierce.[12] Pierce rewrote the LabVIEW program to keep a nearly constant plenum pressure. For the similar conditions 517 kPa (75 psi) in the plenum chamber with proper K_p=0.005 and K_i=1.75) as in the simulation, the actual pressure history during a run is shown in Fig. 3.4. Around 20 s of stable plenum pressure at 517 kPa (75 psi) is observed.

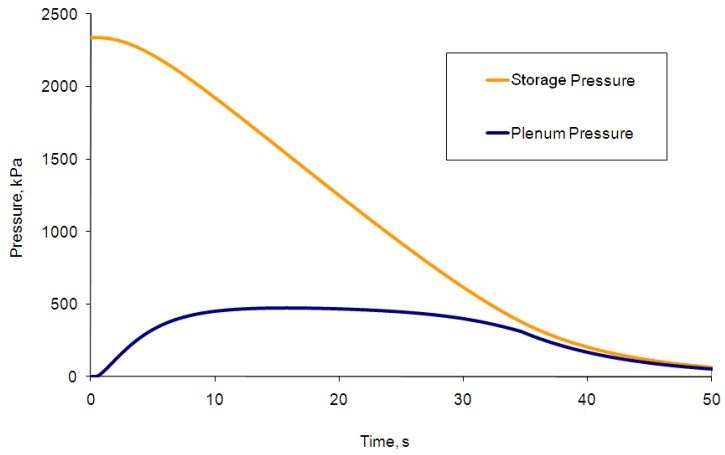

Figure 3.2. Storage and plenum pressure vs time, Mach 2.5 simulation (improper value $K_p = 0.3$).

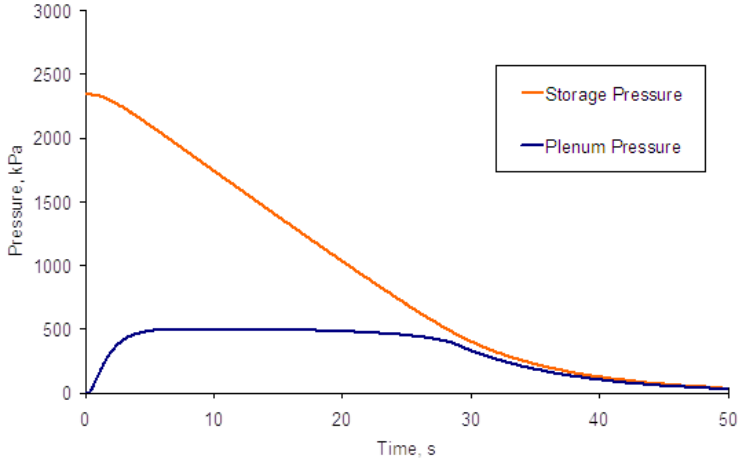

Figure 3.3. Storage and plenum pressure vs time, Mach 2.5 simulation (improper value $K_p = 0.3$).

3.1.2 Test section mach number correction

Another issue of tunnel operation is to ensure that the desired test section Mach number of 2.5 is achieved. Theoretically, one can determine the throat area from the area-Mach number relation

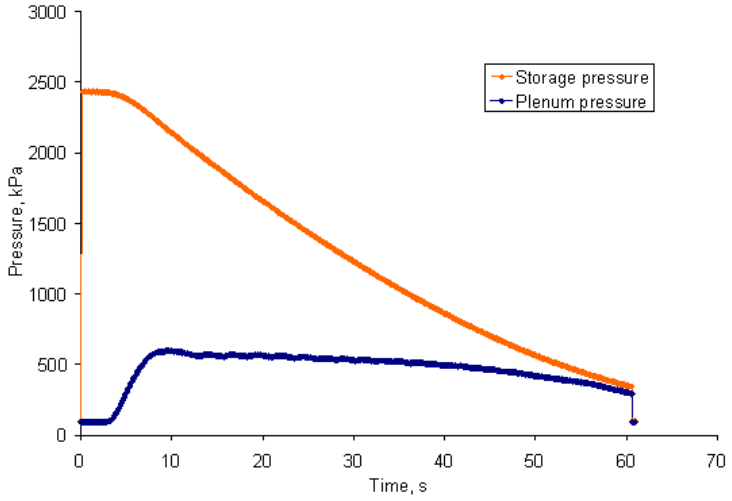

Figure 3.4. Plenum and stroage pressure history at Mach 2.5 with initial storage pressure = 2.34 and plenum set pressure = 517 kPa (proper $K_p = 0.005$ $K_i = 1.75$).

$$\left(\frac{A}{A^*}\right)^2 = \frac{1}{M^2}\left[\frac{2}{\gamma+1}\left(1+\frac{\gamma-1}{2}M^2\right)\right]^{\frac{\gamma+1}{\gamma-1}} \tag{3.1}$$

where the Mach number for the present experiments is 2.5 and where the cross-sectional area of the test section is 15.2 cm^2. Therefore, the throat area from Eqn. 3.1 is 5.77 cm^2. Based on this calculation of throat area, the variable nozzle was adjusted to produce a throat area of 5.77 cm^2. After adjustment, Pierce[12] measured the Mach number in the test section around 2.4 with an accuracy of $\pm 2\%$.

3.1.3 Sealing

A well-sealed test section is necessary to prevent leaks from gaps that can adversely affect the test surface. GE Max 5000 gel was for sealing the test section. Figure 3.5 shows some of the gaps between the windows and the side plates sealed by GE Max 5000 gel. In many cases, GE Max 5000 gel was applied to the windows, side plates, and frames before assembly. Another important place where leaks can be serious are the contact surfaces between the test section and the diffuser. By leaving

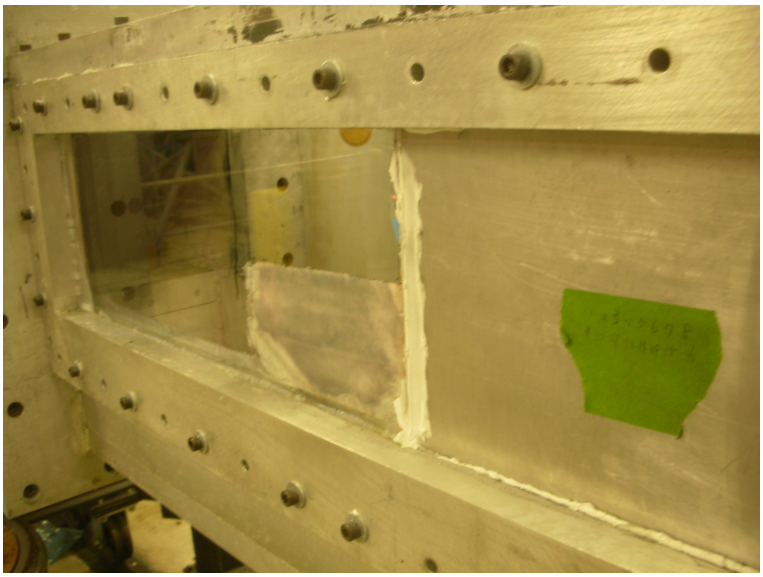

Figure 3.5. GE Max 5000 gel applied to the gaps.

the GE Max 5000 gel in the gap, an elastic gasket was formed to provide a good seal when these two pieces are assembled (Fig. 3.6). By using RISK REACTOR fluorescent liquid, the leaks can be easily found. During a run, the test section was at lower pressure than ambient so any fluorescent liquid applied outside the test section entered the test section through tiny, unexpected gaps. UV light then revealed these leaks. For example, Fig. 3.7 shows a leak through a small gap which was improperly sealed between the side plate and the test section at the lower right corner of the test section surface.

3.1.4 Pressure data processing

Usually, a minimum of 15 s run time was necessary to collect enough 10 data per channel. Data from the first several seconds and of the last few seconds, corresponding to start up and shut down of the tunnel were rejected (see 3.1.1).

The procedure for processing a channel is as follows:

1. Convert PSIG into PSIA.

Figure 3.6. The gasket of GE Max 5000 gel.

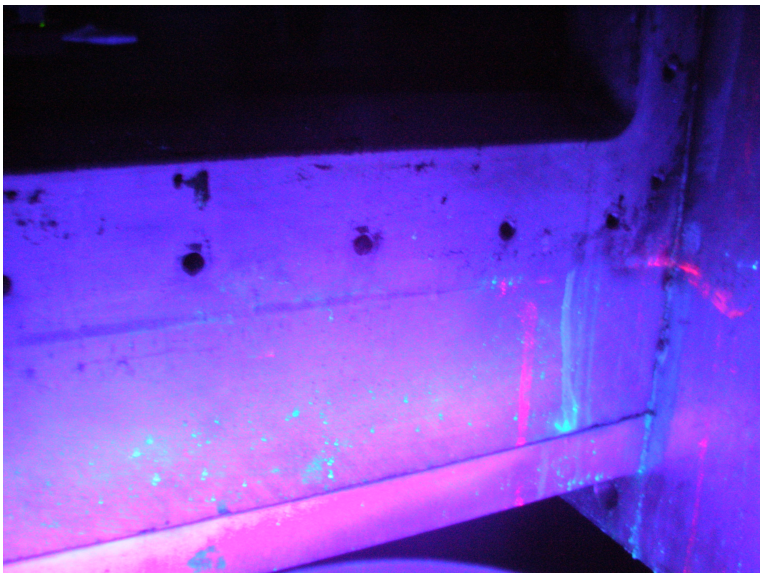

Figure 3.7. Flourescence track pattern under UV light.

2. Normalize P_n, by the reference value P_1, where n = 1, 2,, 16 represent the 16 channels.
3. For every P_n, select ten data between13th and 20th s, average these ten data to form P_n.

4. Plot the pressure ratio against the tap (channel) location for all 16 taps (Fig. 4.1–4.5). Therefore, in the example, 1.34 would be the first point in 45MVG+Flat S (Fig. 4.2(a)).

From 1), 2), and 3), the pressure ratio of a specific tap to the reference tap would be

$$\frac{1}{10}\sum_{k=1}^{10}\frac{P_{n,k}+14.7}{P_{1,k}+14.7} \tag{3.2}$$

where k=1,2,3,,10 represent those ten data of $P_{(n,k)}$. Take the pressure data of 45MVG+Flat for example, for the pressure tap No. 2, if the ten pressure data are selected from 9.948 s to 14.46 s. Thus, the selection of the time range of ten data could be a deviation of this calculation.

CHAPTER 4

RESULTS

4.1 Mean pressure results of all configurations

The following five sections (4.1.1–4.1.5) show the results of mean pressure measurements of six different kinds of configurations. They are "All Flat", "NoMVG+Ramp", "70MVG+Flat", "70MVG+Ramp", "45MVG+Flat", and "45MVG+Ramp". All the results are repeatable. In figures 4.1–4.5 the configurations and the pressure taps are displayed below the pressure distribution. The label nC represents tap 2C, 3C, ,16C from left to right, so does nS. Note that, in 4.1(a), the configuration of All Flat is not shown. Also, the origin is set at the trailing point of the MVG.

4.1.1 "All Flat" and "NoMVG+Ramp" (Baseline)

These two configurations are without the MVG array. Note that the pressure distributions C and S are so close to each other for both the "All Flat" and the "NoMVG+Ramp" configuration. In fact, there is a total of four distributions in Fig. 4.1(a), but only two can be distinguished. For the "All Flat" configuration, there appears to be a slight adverse pressure gradient from tap No. 1 to the region covered by taps No. 2-9 (1.44 mm 35.25 mm). After that, the pressure decreases so that there appears to be a slight favorable gradient. For the "NoMVG+Ramp," the surface pressure ratio from taps No. 2-9 are similar to those on the bare flat plate, with values between 1.04-1.18 before the oblique shock, except that the pressure at tap No. 5 is lower. The inviscid pressure ratio of 1.37 for the 5° ramp at Mach 2.4 is shown in Fig.4.1(a). Note that the boundary layer is unseparated in this case. Figure 4.1(a) shows that the surface pressure does not immediately rise to this value. Instead, the

figure shows that the surface pressure ratio reaches a value of 1.28 and then decreased downstream. In Fig. 4.1(b), Li and Liu's[2] simulation is used for as a reference for

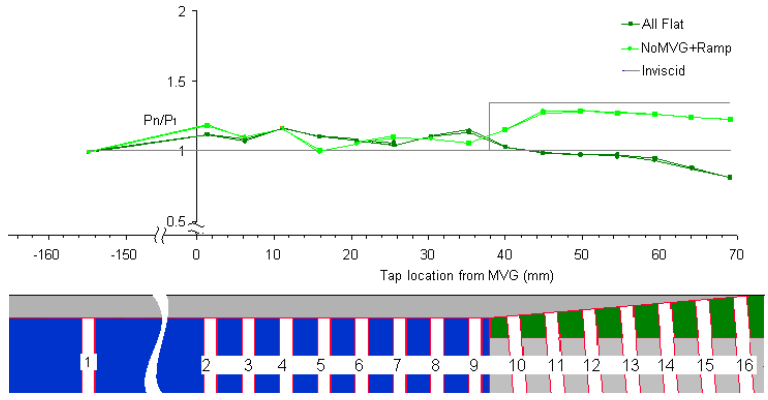

(a)

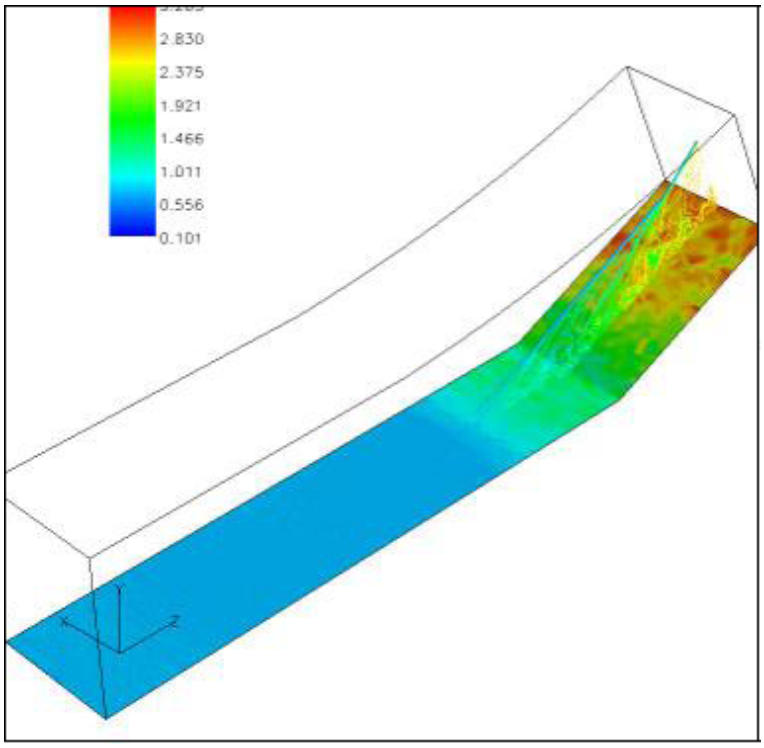

(b)

Figure 4.1. Results of "All Flat" and "NoMVG+Ramp" (a) Pressure measurements and (b) Li and Liu's simulation with "NoMVG+Ramp".

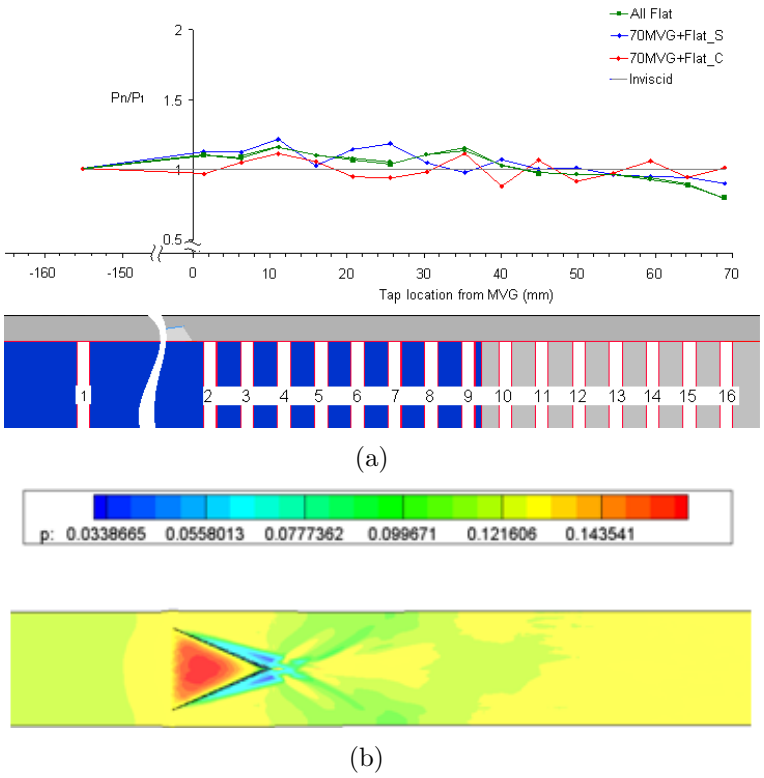

Figure 4.2. Results for "70MVG+Flat" (a) Pressure measurements and (b) Li and Liu's simulation".

shock behavior. (Note that Li and Liu's ramp angle is 24.) We focus on their shock area (shown in green). This area is going to be compared in Figs. 4.3(a) and 4.3(b).

4.1.2 "70MVG+Flat"

In Fig. 4.2(a), pressure distribution C (the pressure taps lined up to the center line of MVG) is lower than pressure distribution S (the pressure taps 1.52 cm (0.6 in.) away from the centered one) before tap 9C and 9S (35.25 mm), except tap 5C and 5S. This means the surface velocity behind MVG is higher than surface velocity between two MVGs. Then, pressure distributions C fluctuates when it goes to downstream. The fluctuation becomes more between tap No.8-12, and then reduces. Compare to pressure distribution C, pressure distribution S is not as fluctuant. According to Li and Liu,[1] vortex pairs are generated at the trailing edge of the MVG, and

our pressure distribution C is right in the middle of the vortex pairs and pressure distribution S is just next to the right vortex, if looking downstream. The fluctuation of pressure distributions C and S is supposed to be related to the behaviors of these vortex pairs up to a certain degree. Figure 4.2(a), Li and Liu[1] also claimed that there should be a high pressure spot behind 70MVG but it seems there is no such spot on pressure distribution C. All we observed is a relative higher pressure area around tap 4C.

4.1.3 "70MVG+Ramp"

For the "70MVG+Ramp" (Fig. 4.3(a)), we found that the pressure distributions C and S have two humps from tap No. 2-9. However, there is no ramp in the baseline. Besides, these two distributions are different all the way to tap No. 16. Moreover, in Li and Liu's[2] simulation (Fig. 4.3(b)), the presence of the MVG caused the high pressure behind the ramp shift a bit forward upstream than without the MVG and also the green pressure area is reduced (Fig. 4.3(b)). These observations can be compared qualitatively with the present results. In distribution C, the value P_9/P_1 =1.05 for the "NoMVG+Ramp" case (Fig. 4.1(a), baseline) which is smaller than the value of P_9/P_1 =1.12 in the "70MVG+Ramp" case (Fig. 4.3(a)). The P_{10}/P_1 =1.15 in the "NoMVG+Ramp" (Fig. 4.1(a), baseline) is lower than the P_{10}/P_1 =1.43 in the "70MVG+Ramp" case (Fig. 4.3(a)). These results are similar to Li and Liu's[2] simulation.

4.1.4 "45MVG+Flat"

In Fig. 4.4, for case "45MVG+Flat", pressure distribution C is no longer below pressure distribution S, before tap No.9C and No.9S, except tap No.2C and No.3C. Instead, it is higher than pressure distribution S. Therefore, the surface velocity is in fact higher at side pressure taps S. After No.9C, pressure distribution C fluctuates

a bit as increasing downstream distance, but not as fluctuant as pressure distribution C does in case "70MVG+Flat." The other important result in this case is that two pressure distributions C and S are initially separated from each other but are tended closer with increasing downstream distance. This result trends to the result

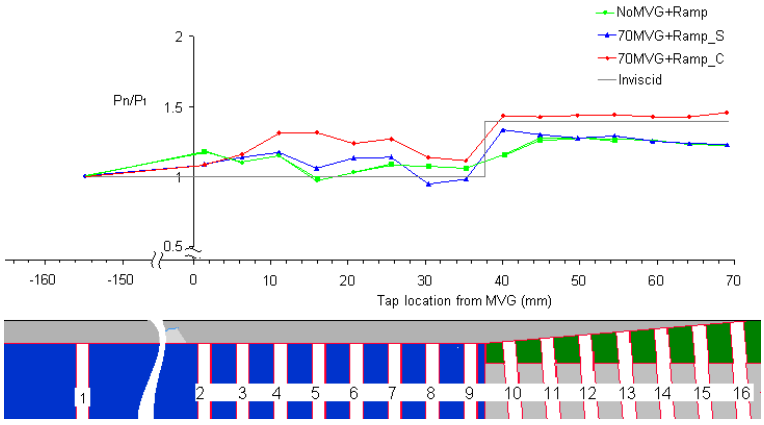

(a)

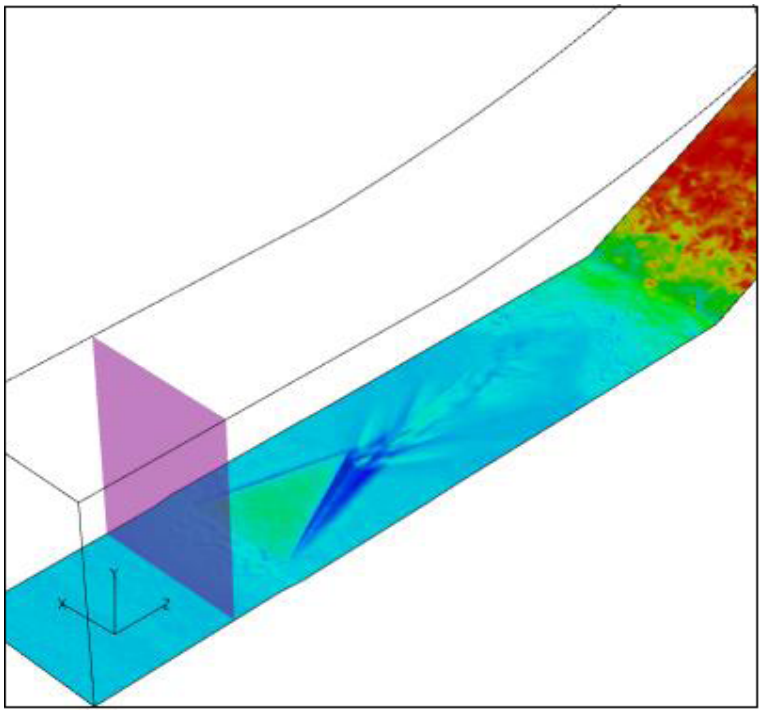

(b)

Figure 4.3. Results for "70MVG+Ramp" (a) Pressure measurements and (b) Li and Liu's simulation".

of baseline, because the two pressure distribution C and S are overlapped in baseline. However, the different result was observed in "70MVG+Flat", that is, pressure distribution C and S are more separated.

4.1.5 "45MVG+Ramp"

In Fig. 4.5, the pressure ratio P_9/P_1 =1.32 at tap No.9C and P_9/P_1 =1.09 at tap No.9S. It seems that the mean shock position has moved a bit forward upstream and again, like the case in "70MVG+Ramp," the pressure at 9C is not the same as the pressure at 9S. Besides, the pressure ratios are low at tap No.8 (P_8/P_1 =0.86 at 8C and P_8/P_1 =0.89 at 8S). The pressure distribution C in this case has only

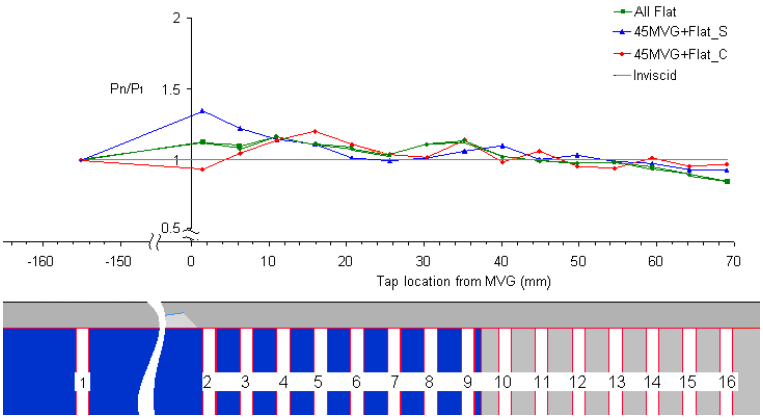

Figure 4.4. Results for "45MVG+Flat".

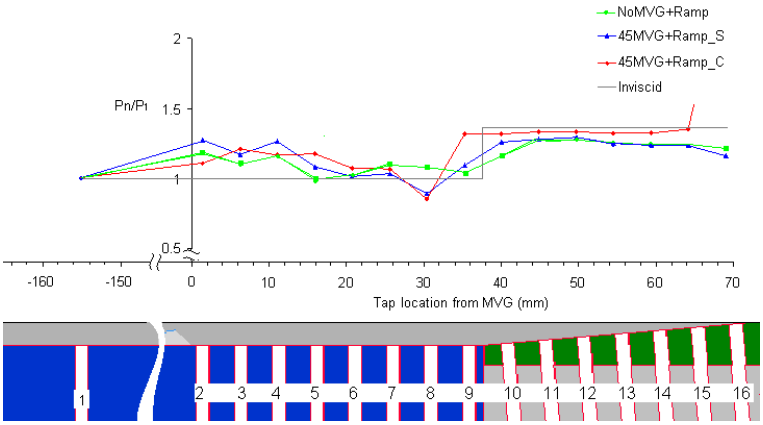

Figure 4.5. Results for "45MVG+Ramp".

one hump, but in "70MVG+Ramp," the pressure distribution of C has two humps. Similar to MVG+Flat cases, the pressure distributions C and S are closer to each other compared to that of in "70MVG+Ramp" (See 4.1.3). The trailing angle seems to play an important role, as we can see the difference between their pressure results.

Some observations can be made:

1. Pressure at tap No.2C is always lower than pressure at tap No.2S, in all 70MVG and 45MVG cases (It still holds in "70MVG+Ramp," where P_2/P_1 =1.08 for 2C and P_2/P_1 =1.09 for 2S). The tap No.2C is right next to MVG at 1.44 mm, so the speed over that area is expected slower than the speed of the high speed region around tap No.2S. Slower speed means the higher pressure. Therefore, the pressure at tap No.2C was expected higher than that of No.2S. However, the result shown a totally opposite situation. We suggest that: (i) For the pressure at tap No.2C lower than the pressure at tap No.2S, it might be because the pressure drops (maybe due to an expansion) at such a tiny distance to MVG. (ii) For the pressure at tap No.2S is higher than the pressure at tap No.2C, this may be due to the two small shock waves originating from the right and left MVGs of S envelop the tap No.2S. After tap No.2C and No.2S, pressure distribution C is usually above the pressure distribution of S, except "70MVG+Flat."
2. All pressure distributions of "All Flat," "70MVG+Flat," and "45MVG+Flat" trend decreasing as increasing downstream distance. This indicates that the surface velocity of downstream is faster than the surface velocity of upstream.
3. Pressure distributions C and S of 70MVG are more separated from each other than those of 45MVG. It seems to indicate that the mixing flow ability of 70MVG is greater than that of 45MVG. Also, based on Li and Liu's [2] simulation, the vortex pairs in 45MVG case are more separated from each other and stay lower to the wall. Their argument may be applied to this pressure result.

4. In shock area, pressure distributions C and S of "70MVG+Ramp" are more separated away from each other than those of 45MVG. It seems to give a hint that that shock wave has been distorted in both case and it distorted more in "70MVG+Ramp." According to Li and Liu's[2] simulation of the more separated vortex pairs and staying lower to the wall in 45MVG case, this may explain the separation degree of pressure distributions C and S in shock area.
5. Results show that all pressure distributions C and S of 70MVG fluctuate more than those of 45MVG. In fact, Li and Liu's[2] simulation claimed that the streamwise vortex separate for more distance from each other in 70MVG when compared to 45MVG. There might be some connections between these fluctuated pressures and their claim.
6. Referring to 5) and Li and Liu's[2] simulation. Our experiments show the pressure ratio starts raising at tap No.8 in "45MVG+Ramp," however, the pressure ratios tend to increase at tap No.9 in both "70MVG+Ramp" and the baseline. The questions would be i) Does that imply that the mean shock position move forward upstream in "45MVG+Ramp"? So does "70MVG+Ramp"? Contrast with baseline. ii) Does it cause by the denser streamwise vortex which 45MVG generates?

CHAPTER 5

CONCLUSION AND FUTURE WORK

Experiments were performed with a baseline flat plate and also with two MVG configurations (70 and 45 trailing edge) mounted ahead of a 5 ramp. The results appeared similar to the simulations reported by Li and Liu.[1],[2]. Three conclusions can be made in present research:

1. The different behaviors of SBLI, with MVG and without MVG, were observed from mean pressure measurements.
2. The mean pressure right behind an MVG is lower than that the middle of two MVGs.
3. The trailing angle of MVG does affect the mean pressure distribution.

The 5 ramp produces an unseparated flow at Mach 2.5. Hence, future work would be to include a ramp of higher angle to achieve flow separation. Furthermore, the pressure fluctuation around the SBLI area is of interest.

APPENDIX A

THE CAD MODEL (ENGINEERING DRAWING BY Pro/ENGINEER)

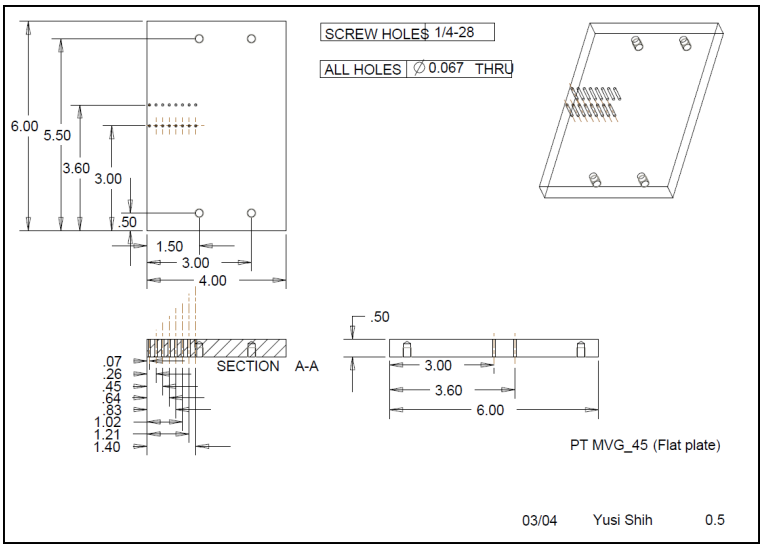

Figure A.1. Pressure taps on MVG plates (Upstream flat plate).

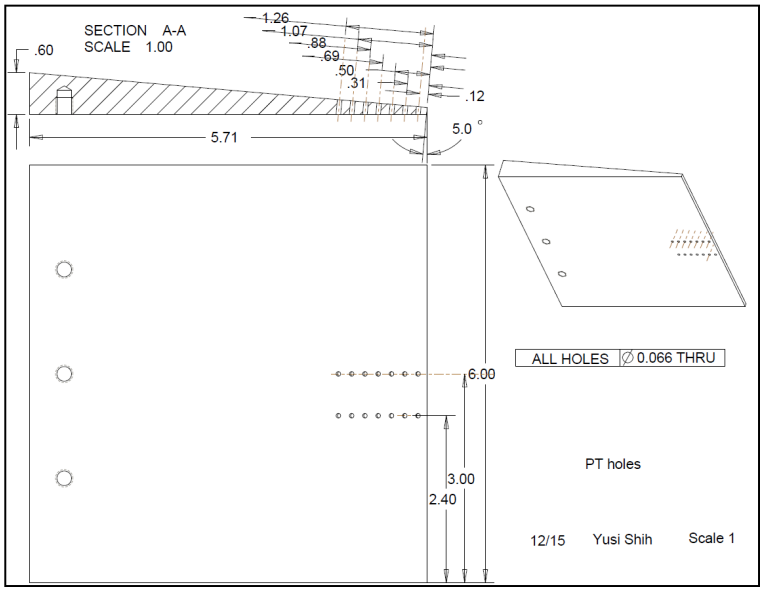

Figure A.2. Pressure taps on ramp segment.

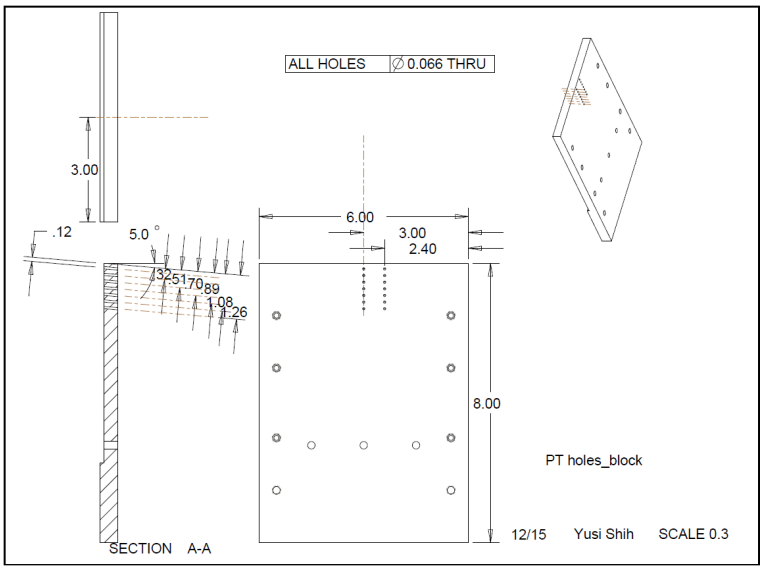

Figure A.3. Pressure taps the base of ramp segment.

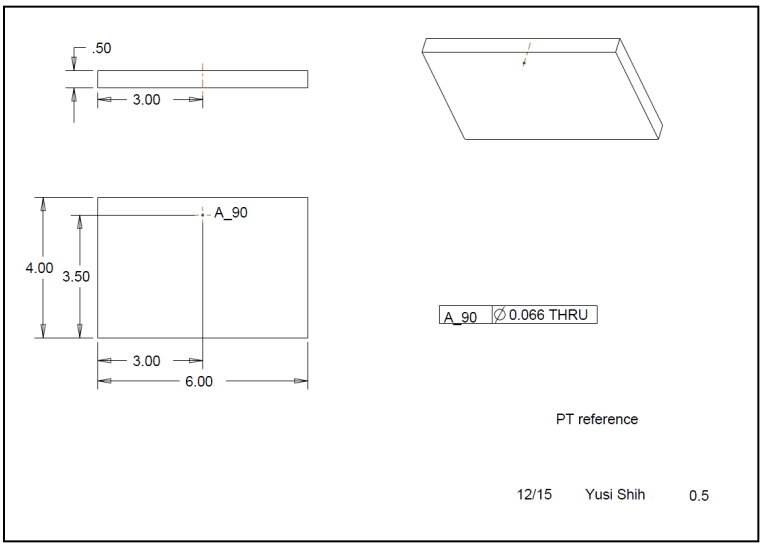

Figure A.4. Reference pressure tap on front plate.

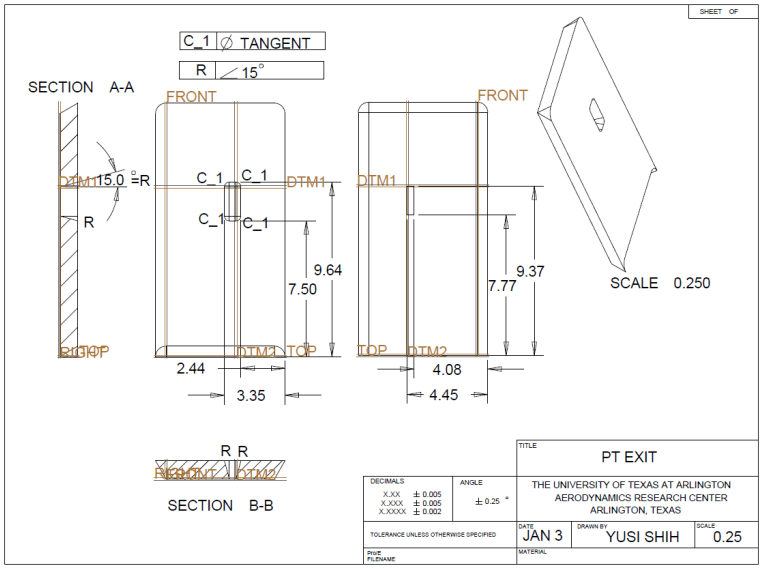

Figure A.5. Access on side plate.

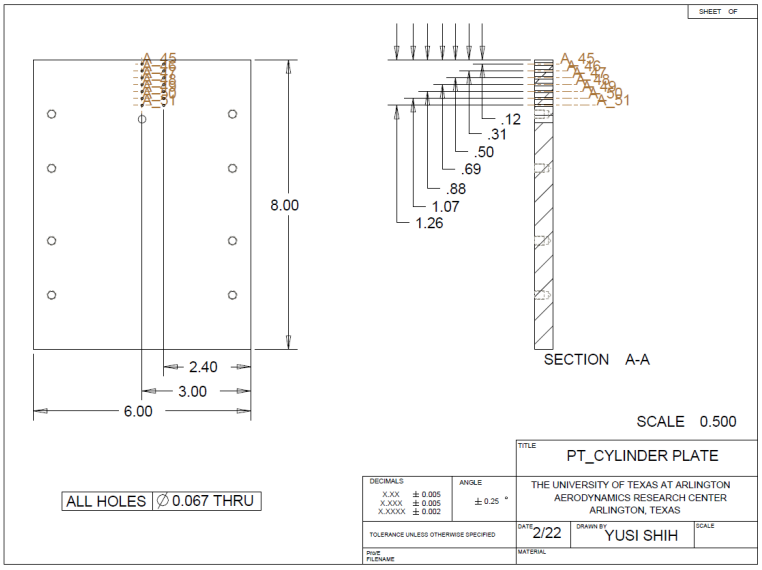

Figure A.6. Pressure taps downstream flat plate.

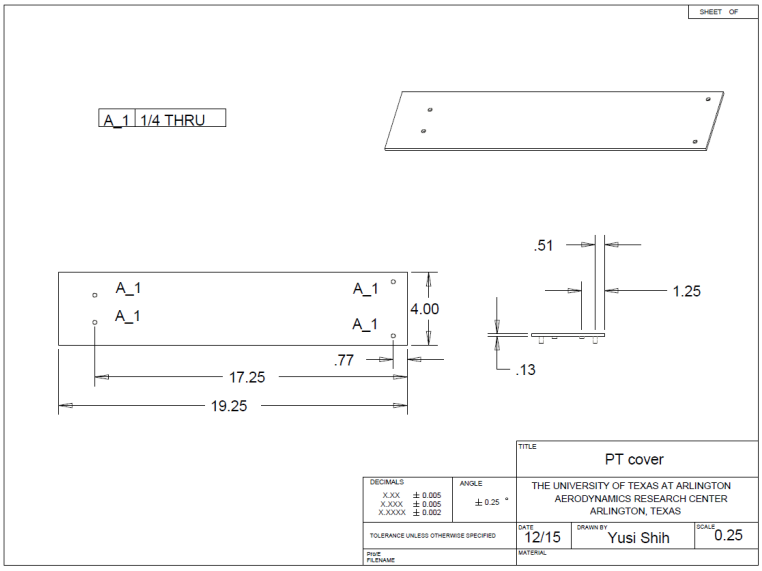

Figure A.7. Cover plate.

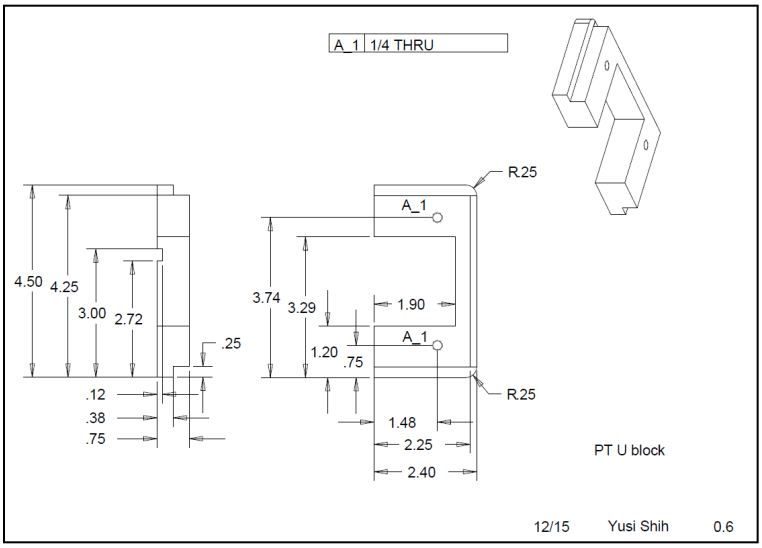

Figure A.8. U shape plate and its small access for reference pressure hole.

REFERENCES

[1] Q. Li and C. Liu, "LES for Supersonic Ramp Control Flow Using MVG at M=2," in *48th AIAA Aerospace Sciences Meeting*, Orlando, Florida, 2010.

[2] ——, "Numerical Investigations on the Effects of the Declining Angle of the Trailing-Edge of MVG," in *48th AIAA Aerospace Sciences Meeting*, no. January, Orlando, Florida, 2010, pp. 1–14.

[3] H. Holden and H. Babinsky, "Effect of Microvortex Generators on Separated Normal Shock/Boundary Layer Interactions," *Journal of Aircraft,*, vol. 44, no. 1, pp. 170–174, 2007.

[4] B. Anderson, J. Tinapple, and L. Surber, "Optimal Control of Shock Wave Turbulent Boundary Layer Interactions Using Micro-Array Actuation," in *3rd AIAA Flow Control Conference*, San Francisco, California, 2006.

[5] P. Ashill, "Research at DERA on Sub Boundary Layer Vortex Generators (SBVGs)," in *39th Aerospace Science Meeting and Exhibit*, no. January, Reno,Nevada, 2001.

[6] P. Ashill, J. Fulker, and K. Hackett, "A Review of Recent Developments in Flow Control," *The Aeronautical Journal*, pp. 205–232, 2005.

[7] P. L. Blinde, R. A. Humble, B. W. V. Oudheusden, and F. Scarano, "Effects of micro-ramps on a shock wave / turbulent boundary layer interaction," *Shock Waves*, no. 19, pp. 507–520, 2009.

[8] R. Bur and D. Coponet, "Separation Control by Vortex Generator Devices in a Transonic Channel Flow," *Shock Waves*, no. 19, pp. 521–530, 2009.

[9] H. Babinsky, Y. Li, and P. Ford, "Microramp Control of Supersonic Oblique Shock-Wave/Boundary-Layer Interactions," *AIAA Journal*, vol. 47, no. 3, pp. 668–675, 2009.

[10] D. McCormick, "Shock-Boundary Layer Interaction Control with Low-Profile Vortex Generators and Passive Cavity," 1992.

[11] H. A. Holden and H. Babinsky, "Vortex Generators Near Shock / Boundary Layer Interactions," in *42nd AIAA Aerospace Science Meeting and Exhibit*, no. January, Reno,Nevada, 2004.

[12] A. Pierce, "Experimental Study of Micro-Vortex Generators at Mach 2.5," Ph.D. dissertation, University of Texas at Arlington, 2010.

[13] J. Matsumoto, "Design and Testing of a Subscale Supersonic Aeropropulsion Wind Tunnel," Ph.D. dissertation, University of Texas at Arlington, 2000.

[14] F. Lu, "Fin Generated Shoc-Wave Boundary -Layer Interactions," Ph.D Dissertation, Pennsylvania State University, 1988.

[15] "Model 9116 Ethernet Intelligent Pressure Scanner User's Manual 2nd Edition," 2007.

[16] Y. Fung and G. S. Settles, "Microprocessor Control of High Speed Wind Tunnel Stagnation Pressure," in *AIAA Aerodynamic Testing Conference*, San Diego, Callifornia, 1988.

[17] E. M. Braun, F. K. Lu, P. K. Panicker, R. R. Mitchell, D. R. Wilson, and J. C. Dutton, "Supersonic Blowdown Wind Tunnel Control Using LabVIEW," in *46th AIAA Aerospace Sciences Meeting and Exhibit*, no. January, Reno,Nevada, 2008, pp. 1–14.

[18] H. Babinsky, N. J. Makinson, and C. E. Morgan, "Micro-Vortex Generator Flow Control for Supersonic Engine Inlets," in *45th AIAA Aerospace Sciences Meeting and Exhibit*, no. January, Reno,Nevada, 2007, pp. 1–8.

[19] F. K. Lu, "An Experimental Study of Three-Dimensional Shock-Wave Boundary Layer Interactions Generated by Sharp Fins," Masters Thesis, Princeton University, 1983.

[20] V. Speaker, "Spectra and Space-Time Correlations of the Fluctuating Pressures at a Wall Beneath a Supersonic Turbulent Boundary Layer Pertubed by Steps and Shock Waves," 1966.

BIOGRAPHICAL STATEMENT

Yusi Shih was born in Taiwan and has a traditional family. He likes to spend time with friends, meet new people, and travel around the world. He is also a fan of Bill Gates, Albert Einstein, and Scarlett Johansson. He is especially interested in space tourism and hope that he can work for it in his future career.